Available online at www.sciencedirect.com
SCIENCE DIRECT®
International Journal of Heat and Mass Transfer 48 (2005) 2050–2063
International Journal of HEAT and MASS TRANSFER
www.elsevier.com/locate/ijhmt

Effects of ridged walls on the heat transfer in a heated square duct

M. Salinas Vázquez [a,*], W. Vicente Rodríguez [a], R. Issa [b]

[a] Instituto de Ingeniería, UNAM, Coordinacion de Ingenieria de Procesos Industrails Y Ambientales, Circuito Interior, Ciudad Universitaria, 04510 México DF, México
[b] LEGI-MOST, INPG, BP 53X, 38041 Grenoble Cedex 9, France

Received 23 April 2004
Available online 16 March 2005

Abstract

Turbulent flows in rectangular cooling ducts of rocket engine thrust chambers are characterized by secondary motions of Prandtl's first and second kinds. These secondary currents play a prominent part in heat transfer between the thrust chamber and the cooling gas conveyed in the duct. Previous numerical and experimental works reveal that attaching ridges on the walls of the duct causes the formation of new secondary flows of Prandtl's second kind. These new structures are likely to increase the heat transfer. The present study has investigated numerically, through large eddy simulations, the effect of different forms of ridges on heat transfer in straight square duct flows.

Keywords: Duct; Heated; Ridge; LES

1. Introduction

In rocket engine thrust chambers, temperature and heat transfer could respectively exceed 3500 K and 100 MW m^{-2}. This excessive heat must obviously be evacuated in order to keep the temperature of the walls in the thrust chamber under the fusion point of the material.

Previous numerical investigations on heated straight ducts characterized by a square cross-section have been reported in Salinas Vázquez and Métais [1], considering that the temperature T_h imposed on a wall was higher than the temperature T_w imposed on the three other walls. These studies reveal that, in the vicinity of the corners, relative to the hot wall plane, the reinforcement of secondary flows of Prandtl's second kind creates an impingement of the heated wall by the cold fluid coming from the core duct. Whereas, near the middle hot wall plane, the creation of a quasi-stationary big ejection decreases the mean wall heat flux. This phenomenon can be observed in Fig. 1 which represents the distribution of the mean normal to the wall heat flux along the hot wall, defined by:

$$q_w = [\langle\kappa\rangle\partial\langle T\rangle/\partial n]_w \quad (1)$$

where $\langle\kappa\rangle$ is the mean thermal conductivity, $\langle T\rangle$ the mean temperature and n designates the normal direction to the wall. q_w is normalized by the mean bulk wall heat flux on the hot wall (q_w^a). Moreover, the latest big ejection, which can be visualized from the instantaneous fields of temperature (contours) and transverse velocity (vectors) in Fig. 1, concentrates the turbulence

* Corresponding author.

0017-9310/$ - see front matter © 2005 Elsevier Ltd. All rights reserved.
doi:10.1016/j.ijheatmasstransfer.2004.10.036

Nomenclature

b	minor ridge base, m
B	mayor ridge base, m
C_f	skin friction
C_k	Kolmogorov constant
C_v	specific heat constant volume, J kg^{-1} K^{-1}
$C_{\mu f}$	Constant structure function model
D_h	hydraulic diameter, m
e	total energy, J
f	body force, kg m^{-2} s^{-2}
$\widetilde{F_i}$	flux, compressible conservative equation
$\widehat{F_2}$	structure function, m^2 s^{-2}
Gr	Grashof number
H	ridge high, m
I	ridge spacing, m
k	thermal conductivity, W m^{-1} K^{-1}
M	Mach number
n	normal direction
P	pressure, Pa
Pr	Prandtl number,
q_w	heat flux, W m^{-2}
R	particular constant ideal gas, J kg^{-1} K^{-1}
Re	Reynolds number
S	source term
S_{ij}	deviatoric part of the strain rate, s^{-1}
t	time, s
T	temperature, K
T_w	wall temperature, K
T_h	high wall temperature, K
T_{rms}	fluctuating temperature mean root square, K
u	longitudinal velocity, x-direction, m s^{-1}
$\vec{u}$	velocity vector, m s^{-1}
U	longitudinal mean velocity, x-direction, m s^{-1}
$\mathbf{U}$	conservation equations vector,
U_b	longitudinal bulk velocity, x-direction, m s^{-1}
u'	fluctuating longitudinal velocity, x-direction, m s^{-1}
u_{rms}	fluctuating longitudinal velocity mean root square, x-direction, m s^{-1}
u_τ	friction velocities, $(\tau\rho^{-1})^{1/2}$, m s^{-1}
$\langle u'T'\rangle$	turbulent heat flux in x-direction, K m s^{-1}
$\langle \vec{u}'T'\rangle$	turbulent heat flux vector, K m s^{-1}
$\langle u'v'\rangle$	Reynolds stress, m^2 s^{-2}
v	transversal velocity, y-direction, m s^{-1}
$\langle v'T'\rangle$	turbulent heat flux in y-direction, K m s^{-1}
w	transversal velocity, z-direction, m s^{-1}
$\langle w'T'\rangle$	turbulent heat flux in z-direction, K m s^{-1}
W	transversal mean velocity, z-direction, m s^{-1}
x	longitudinal direction, m
$\vec{x}$	spatial vector, m
x_i	spatial directions, m
y	transversal direction, m
y^+	wall units, $(\mu\rho^{-1}u_\tau^{-1})$
z	transversal direction, m

Greek symbols

μ	viscosity, N s m^{-2}
γ	specific heats ratio
δ_{ij}	Dirac function,
v_t	turbulent viscosity, m^2 s^{-1}
Δ	mean local grid size, m
ρ	density, kg m^{-3}
ρ_b	bulk density, kg m^{-3}
τ	shear stress, N m^{-2}
τ^α	mean shear stress on the heat wall, N m^{-2}

Subindices

i	three spatial directions, $\forall i \in \{1,2,3\}$
w	at the wall

Superindex

α	bulk value

around the middle wall plane, $z/D_h \approx 0.5$. Concentrated ejections around the middle wall plane also create a low temperature gradient in this zone, decreasing the wall heat flux (q_w), see Fig. 1. From results in square ducts [1], it can also be verified that the reinforcement in size and intensity of mean secondary flows is related to changes in thermal variables. Fig. 2 shows this transformation of the mean secondary flows and its influence over the T_{rms} contours for two different temperatures $T_h/T_w = 1.75$ and $T_h/T_w = 3.25$. For highest T_h values, the ejection zone (dashed line zone) and maximum T_{rms} values zone are more concentrated around the middle wall plane. The zone corresponds to the fluid engulfment (solid line zone) increases in size and the T_{rms} contours are deformed close to the heated wall.

The importance of these results is that we can change the thermal turbulence behavior in cooling ducts by changing the form of the mean secondary flows. Two different sorts of modifications are possible: introducing a curvature in the duct (and consider thus Prandtl's first kind secondary flows) or changing the cross-section of the initial straight square duct.

The study presented in this paper focuses on the second option. These modified secondary motions would supposedly increase energy transport and global heat transfer within the duct. As new geometries, a square

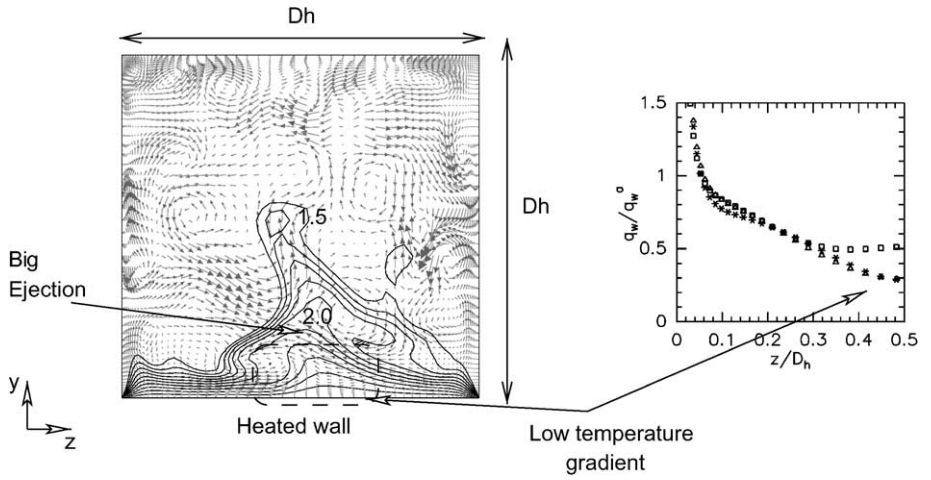

Fig. 1. Instantaneous fields, secondary flows vectors and temperature contours (T/T_w) in a heated square duct (left) and spatial evolution of mean wall heat flux along the hot wall of the square duct (right) [1].

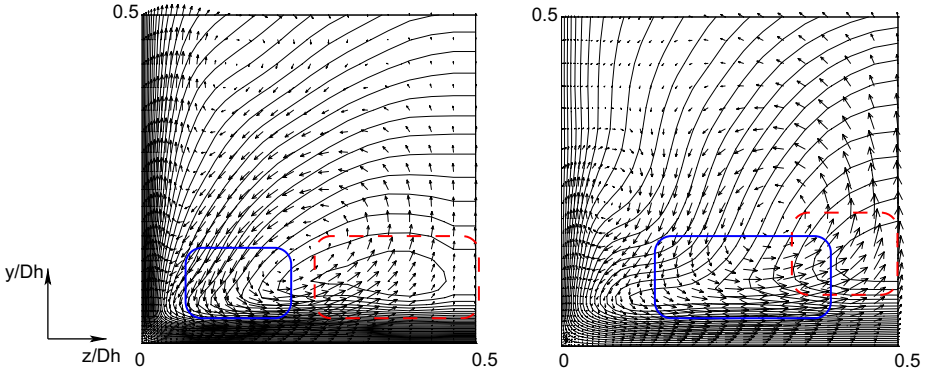

Fig. 2. Mean secondary flows and T_{rms} in the square duct. $T_h/T_w = 1.75$ (left) and $T_h/T_w = 3.25$ (right).

heated duct with different forms of longitudinal ridges on the heated wall are considered and compared by means of large eddy simulations.

In the first part of this paper, results concerning isothermal straight ridged ducts (four walls at the same temperature) are presented. The effect of ridges on the flow is studied. In the second part, the performance of ridges in heated configurations is presented, and finally the influence of the position and dimensions of ridges is discussed.

2. Governing equations and numerical method

2.1. Flow equations

The continuity, compressible Navier–Stokes and energy equations are normalized using the following reference dimensions: bulk velocity U_b, bulk density ρ_b, hydraulic diameter D_h of each duct and a reference temperature T_w applied on duct walls. In the so-called fast-conservation, these equations are:

$$\frac{\partial \mathbf{U}}{\partial t} + \frac{\partial F_i}{\partial x_i} = S \tag{2}$$

U is a five component vector defined by:

$$\mathbf{U} = {}^{\mathrm{T}}(\rho, \rho u_1, \rho u_2, \rho u_3, \rho e) \tag{3}$$

where u_i represents the velocity component in the i direction and e the total energy per unit mass ($e = \rho C_v T + \frac{1}{2}\rho(u_i^2 + u_i^2 + u_i^2)$).

F_i are fluxes in the three spatial directions $\forall i \in \{1,2,3\}$ defined by:

$$F_i = \begin{pmatrix} -\rho u_i \\ -\rho u_i u_1 - \frac{1}{\gamma M^2} p\delta_{i1} + \frac{\mu}{Re} S_{i1} \\ -\rho u_i u_2 + \frac{1}{\gamma M^2} p\delta_{i2} + \frac{\mu}{Re} S_{i2} \\ -\rho u_i u_3 + \frac{1}{\gamma M^2} p\delta_{i3} + \frac{\mu}{Re} S_{i3} \\ -(\rho e + p)u_i + \frac{\gamma M^2}{Re}\mu S_{ij} u_{ij} + \frac{\gamma}{\gamma - 1}\frac{k}{Pr\,Re}\frac{\partial T}{\partial x_i} \end{pmatrix} \tag{4}$$

Re, *M* and *Pr* are respectively the Reynolds, Mach and Prandtl numbers, based on the previous reference dimensions. The gas is considered as an ideal gas: $P = \rho RT$, where R is the particular gas constant.

S_{ij} denotes the deviatoric part of the strain rate tensor defined by:

$$S_{ij} = \left(\frac{\partial u_i}{\partial x_j} + \frac{\partial u_j}{\partial x_i} - \frac{2}{3}(\vec{\nabla}\cdot\vec{u})\delta_{ij}\right) \tag{5}$$

S corresponds to a forcing term, used to offset friction head loss. Its expression is:

$$S = (0, f, 0, 0, \gamma M^2 U_b f) \tag{6}$$

where f is a body force introduced to impose a constant pressure gradient.

2.2. Large eddy simulation

The large eddy simulation (LES) technique is used to compute turbulent effects within the flow. It consists in deterministically simulating the large scales of the flow since they are the most energetic. The small scales are then filtered out but, as kinetic energy transfers occur between small and large scales, they influence the large scale motions [2]. Consequently, small scales effect must be considered through a model.

LES equations are found by applying a high-pass spatial filter $G_{\Delta x}(x)$ of size Δx to the conservation equations. This filtering operation eliminates scales smaller than the filter size Δx, called the sub-grid scales. A new tensor then appears in the Navier–Stokes equations, called the subgrid scale tensor. Physically, it represents the influence of small scales on large scales and must be modeled.

The subgrid scale tensor is modeled through the classical eddy-viscosity assumption, computed from a subgrid-scale model, wherein the selective structure function model is applied [3,4]:

$$\nu_t(\vec{x}, \Delta x, t) = C_{sf}\Delta\sqrt[2]{\widetilde{F_2}(\vec{x}, \Delta, t)} \tag{7}$$

where C_{sf} is linked to the Kolmogorov's constant $C_k : C_{sf} = 0.105 C_k^{-3/2}$. C_{sf} takes the value 0.104 for $C_k = 1.4$.

$\widetilde{F_2}(\vec{x}, \Delta x, t)$ is the second-order velocity structure function, constructed with the instantaneous filtered velocity field. Practically, $\widetilde{F_2}(\vec{x}, \Delta, t)$ is determined by considering an average relative to six neighboring points. Turbulent thermal conductivity is obtained from a constant turbulent Prandtl number, equal to 0.6.

2.3. Resolution method

Filtered equations are solved in generalized coordinates by means of an extension of the fully explicit Mac-Cormack scheme, fourth order in space and second in time [5]. A detailed explanation of LES formalism and numerical schemes used in the present work, and an extended validation of the computational code have been presented in Salinas Vázquez and Métais [1].

3. Computational domains and flow configuration

Dimensions of the four computational domains are equal to those used in a previous work [1]: $12.8D_h \times D_h \times D_h$, respectively in the x (streamwise), y (spanwise) and z (transverse) directions. The streamwise length has also shown that it can ensure the correct representation of the longest turbulent structures present within the flow [1]. Cross-sections of the four computational domains consist of a geometrical square. Three of them are implemented with two ridges on one of the walls (see Fig. 3). Three different forms of ridges are studied, with their geometrical characteristics provided in Table 1. Changes in wet perimeter and area due to the presence of the ridges are negligible. This ridge forms were chosen primarily for their simplicity.

The computational grid consists of $120 \times 60 \times 60$ nodes along x, y and z directions respectively. A non-uniform (orthogonal) grid is used in the y and z directions to correctly simulate the near-wall regions [1]. For ridged duct grids, the same distribution is effected in both transverse and spanwise directions. Due to the ridges small size, no special attention is paid around them.

The Reynolds and Mach numbers are respectively equal to 6000 and 0.5. These numbers are based on reference dimensions presented in Section 2.1. As the Grashoff number is much smaller than one, gravity effects are negligible and therefore not considered.

3.1. Boundary conditions

No-slip boundary conditions are used along all solid walls. Periodic boundary conditions along the streamwise direction x are imposed. Pressure at the wall is obtained by solving the equations of conservation. In the isothermal LES, temperature of each wall is taken equal to the reference temperature (see Section 2.1). In the second part of the study when heat is applied, a temperature T_h is imposed at the ridged wall and the temperature T_w is maintained on the other walls. In the present work, only the ratio $T_h/T_w = 2.5$ was considered.

3.2. Statistics quantities

Mean statistics are obtained by averaging in the homogeneous direction, x, and in time. In ridged sections, statistics are optimized by considering the symmetry plane present in these sections. The bulk quantities

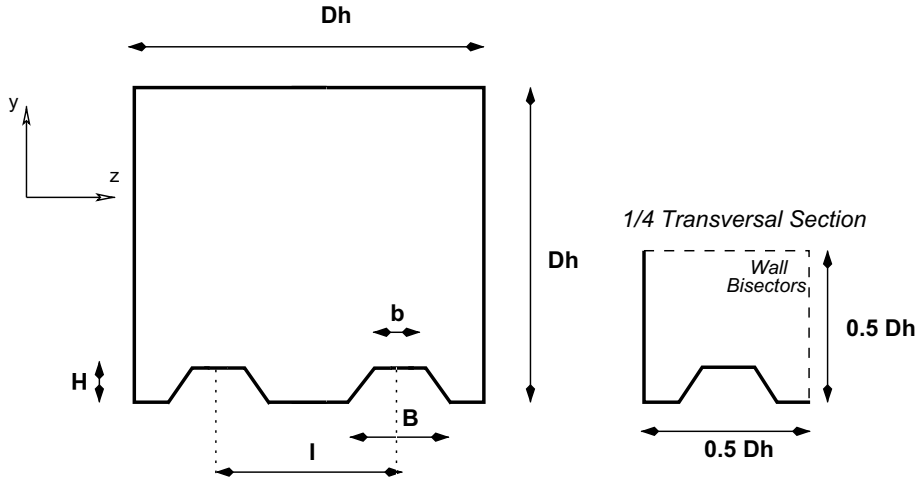

Fig. 3. Cross-section of the ridged duct.

Table 1
Isothermal ridged duct (ridges geometrical characteristics)

Form	H/D_h	B/D_h	b/D_h	I/D_h
Trapezoidal	0.03	0.3	0.1	0.5
Triangular	0.03	0.3	–	0.5
Circular	0.03	0.3	–	0.5

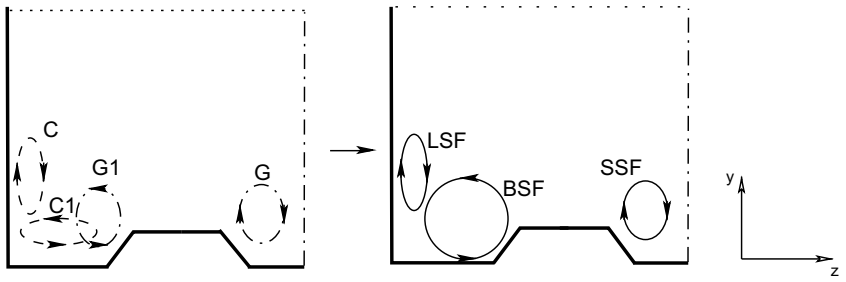

Fig. 4. Repartition of mean secondary flows in a ridged duct. 1/4 transversal section.

refer to the mean quantity averaged along the y- and z-directions. Similar statistics quantities are defined in Salinas Vázquez and Métais [1].

4. Isothermal ridged ducts

4.1. Secondary flow transformations and consequences

Many numerical [6,7,1] and experimental [8–10] investigations concerning turbulent flows in non-circular ducts adduce to the presence of secondary flows of Prandtl's second kind in each corner. These mean motions, due to important gradients of Reynolds stresses, consist of two mean longitudinal vortices, located in a plane perpendicular to the direction of principal flow, see Fig. 5. Since they carry fluid from the center of the duct towards the corner, these motions play an important role in convection of momentum, energy and vorticity.

Some studies about single ribblet [11] and ridged open channels [12,13] have shown that turbulent activity is increased above the ribblet since other secondary flows are created on each side of the ridge.

In the particular case where ridges are implemented on one wall of a square duct, the secondary flows created by them, G and G1, interact with those created by the

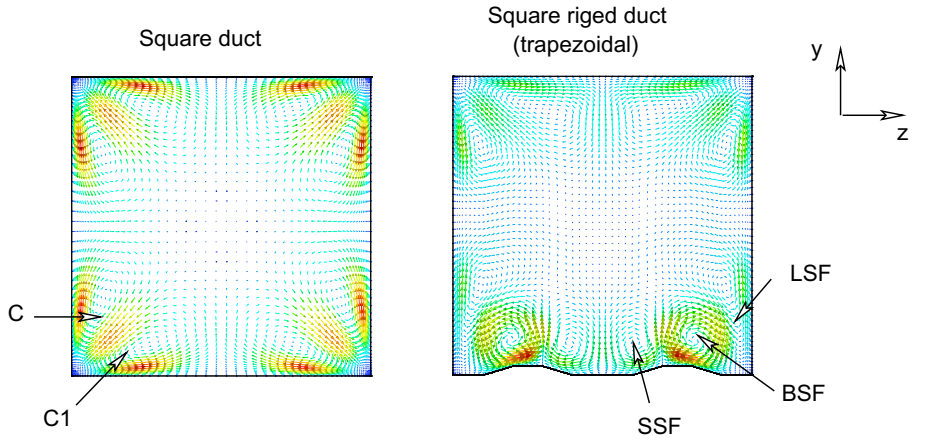

Fig. 5. Mean transversal and vertical velocity field vector in square duct [1] (left) and in trapezoidal ridged duct (right).

corners of the duct, C and C1 [1,6,7]. C1 and G1 merge to form a bigger secondary flow (BSF) (see Fig. 4). The repartition of secondary motions (see Figs. 4 and 5) consists thus of a small secondary flow (SSF) due to the ridge and located around the middle plane of the ridged wall [14,15,12], the previous secondary flow (BSF), and a deformed typical corner secondary flow, lateral secondary flow (LSF). No modification is observed in the secondary flows located in the opposite wall of the duct (PWSF).

Fig. 5 shows the mean transverse and vertical velocity fields for the square duct and the trapezoidal ridged duct. The transformation of C1 in the ridged duct, and the presence of the two weak secondary flows around the middle wall plane (**SSF**) are presented. Similar transformations are observed for the other ridged geometries.

By modifying instantaneous fields and mean secondary motions, the ridges have two important advantages in the thermal performance enhancement: a global escalation of the turbulence (mixing activity) and an increase in the heat transfer normal to the wall around the middle wall plane (critical zone, see Fig. 1) due to the SSFs effect. However, an increase of the streamwise velocity gradient is also observed, similar to the effect noticed in ribblet works [11], when the spacing between ribblets is bigger than the critical drag reduction length. An increase of the wall shear stresses, considered as an undesirable effect, is then found.

4.2. Intensity and position of BSF and SSF

Fig. 6 shows statistical results for four different z-planes ($z/D_h = 0.15$, 0.25, 0.35 and 0.5). Firstly, evolutions of mean spanwise velocity (top) in planes $z/D_h = 0.15$ and $z/D_h = 0.25$ provide the presence of BSF in ridged ducts and C1 in the square duct. A quantitative evaluation of the intensity of these vortices could be done by considering the maximum of mean spanwise velocity, located on a vertical profile connecting to the center of each BSF. Table 2, which assesses the intensity of each vortex under the previous assumption, shows that triangular and trapezoidal ridged ducts induce the most intense BSF.

Evolutions of mean spanwise velocity in plane $z/D_h = 0.35$ reveal the presence of SSF in ridged ducts, and negative spanwise velocity close the wall ($y/D_h = 0.0$). As previously mentioned, Table 2 assesses their intensity. This shows that trapezoidal ridges induce the most intense SSF. An evolution of mean spanwise velocity performed in the center of each SSF shows that they are not dependant on the ridges form. The transversal position obtained for the three ridged duct is coherent with that obtained by Nezu and Nakagawa [12]. These authors expose that this position is equal to $I/4$.

4.3. Influence of ridges on turbulent activity

Fig. 6 also presents the evolution of the Reynolds stresses $\langle u'v' \rangle$ normalized by the mean friction velocity in planes $z/D_h = 0.15$, 0.25, 0.35 and 0.5 (middle). Peaks present on these graphs are the signature of turbulent phenomena as ejections and sweeps, principally [1]. The trapezoidal ridge induces approximately a 44% increase in $\langle u'v' \rangle / u_\tau^2$ in its middle ($z/D_h = 0.25$), in comparison to a square duct in this zone. Ribblets studies have already observed the enhancement of turbulence above isolated elements [11]. In this zone, where BSF is located, the ejections-sweeps activity is very strong, similar than the activity observed around the middle plane of square duct [1]. In the extremity of the ridge close the middle wall plane ($z/D_h = 0.5$), Reynolds stresses are decreased when compared to those in a square duct. For the same trapezoidal ridged duct, the decrease is evaluated as $\approx -40\%$. It could be assumed that in this

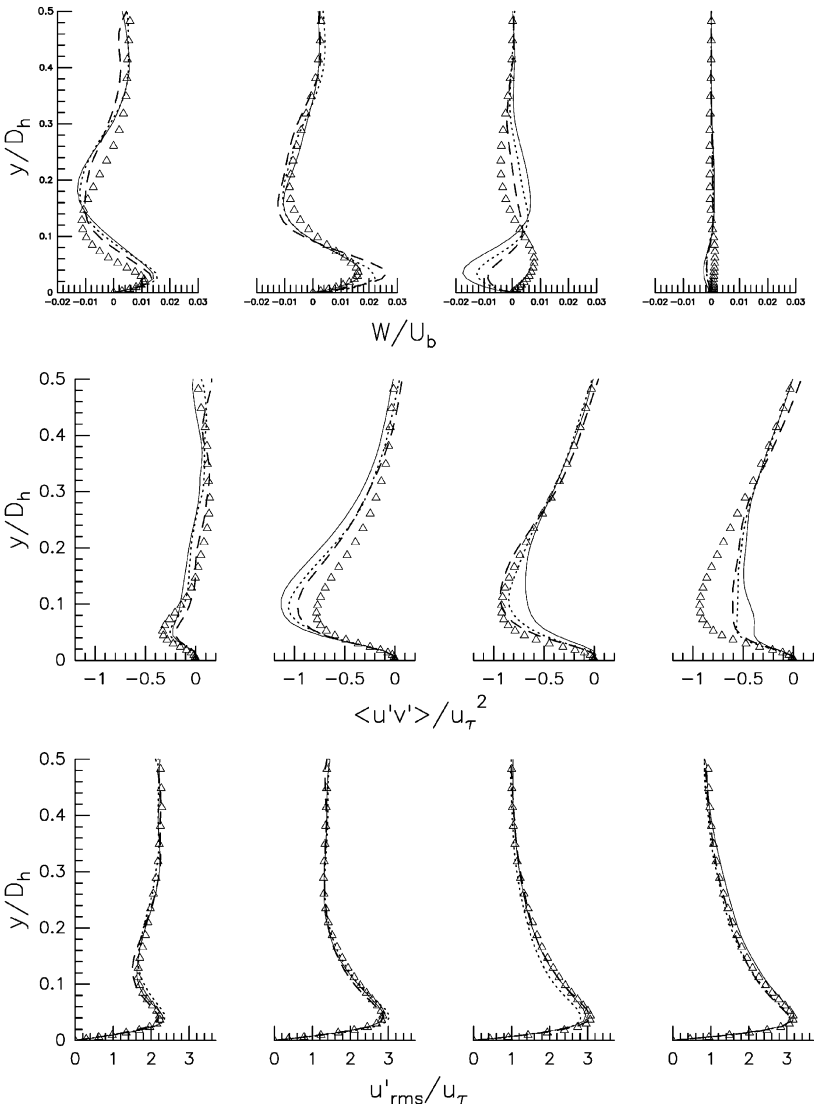

Fig. 6. Isothermal ducts. Comparison between the four ducts for four z-planes $z/D_h = 0.15$, 0.25, 0.35 and 0.5. Values are normalized by the bulk velocity (U_b) for mean spanwise velocity (W), and by friction velocity (u_τ) for Reynolds stress $\langle u'v' \rangle$ and rms of streamwise velocity. Square duct (△); trapezoidal ridged (—); circular ridged (– –); and triangular ridged (···).

Table 2
Isothermal ridged duct (maximal transversal velocity for BSF and SSF)

Type of duct	Maximal W in BSF	Maximal W in SSF
Square duct	1.9% U_b (C1)	–
Trapezoidal ridge	3.2% U_b	1.8% U_b
Circular ridge	3.0% U_b	1.3% U_b
Triangular ridge	3.2% U_b	1.0% U_b

zone of the ridged duct, sweeps (which engulf fluid to the wall) are favored as ejections, which are more energetic. The decrease is more important for the trapezoidal ridged section and this observation is coherent with the fact that a trapezoidal ridge induces a more intense SSF. Indeed, these changes in $\langle u'v' \rangle$, Fig. 6, show that u_{rms} is as intense in ridged ducts as in square duct, for the four z-planes considered. This observation reveals that turbulent activity expressed by Reynolds stresses $\langle u'v' \rangle$ is principally linked to vertical fluctuations.

4.4. Evolution of wall shear stresses

Fig. 7 represents the evolution of wall shear stresses, normalized by its mean bulk value along the wall duct, τ^α, defined by:

$$\tau = [\mu \partial U/\partial n]_w \quad (8)$$

where μ designs the local dynamic viscosity, $\langle U \rangle$ the mean streamwise velocity and n the normal direction to the wall. It was verified that the contribution of other components of the strain rate tensor was weaker.

Peaks in ridged ducts profiles are due principally to the duct geometry and not to an eventual lack of statistics convergence. Peaks of shear stresses relative to ridged duct observed around $z/D_h \approx 0.2$ and at $z/D_h = 0.5$ are direct consequences of BSF's and SSF's actions

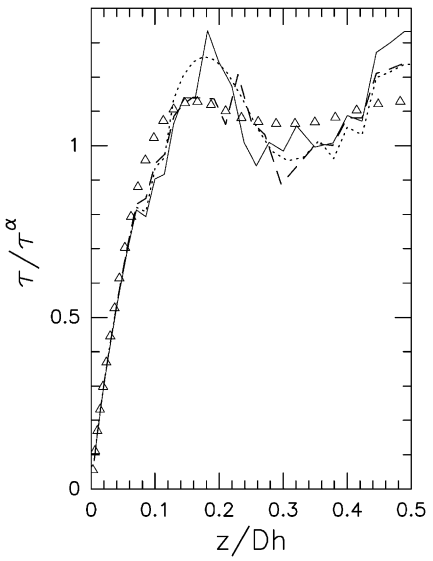

Fig. 7. Spatial evolution of wall shear stresses (normalized by its mean value). Square duct (△); trapezoidal ridged (—); circular ridged (– –); and triangular ridged (···).

Table 3
Isothermal ridged duct (increase of the skin friction (C_f))

Form	c_f^α increase (%)
Trapezoidal ridged	+1.4
Triangular ridged	+1.3
Circular ridged	+1.2

respectively, since these vortices induce important mean streamwise velocity gradients in these zones. Trapezoidal ridged duct induces at $z/D_h = 0.5$ the most important mean bulk skin friction, $C_f^\alpha = \frac{\tau^\alpha}{0.5\rho_b U_b^2}$, due principally to the high intensity of SSF in this duct (see Table 2).

Table 3 provides the mean bulk skin friction coefficient over the ridged wall in comparison with its value obtained in a square duct [1]. A triangular ridged duct induces the most important skin friction coefficient.

5. Heated ridged ducts

The geometrical characteristics of the ridged heated ducts are similar to those of the isothermal ducts. The difference is the imposition of a higher temperature, T_h at the ridged wall. The other three walls have the reference temperature, T_w. Only one case of heated ducts is studied here for three types of ridge form, for a ratio of $T_h/T_w = 2.5$. Statistics are obtained as those in the isothermal ridged duct.

In heated ridged ducts, as in a heated square duct, turbulent activity is characterized by the enhancement of ejections from the heated wall. In the square heated duct, the increase in the size of the ejections above the heated wall and the confinement of secondary flows pro-

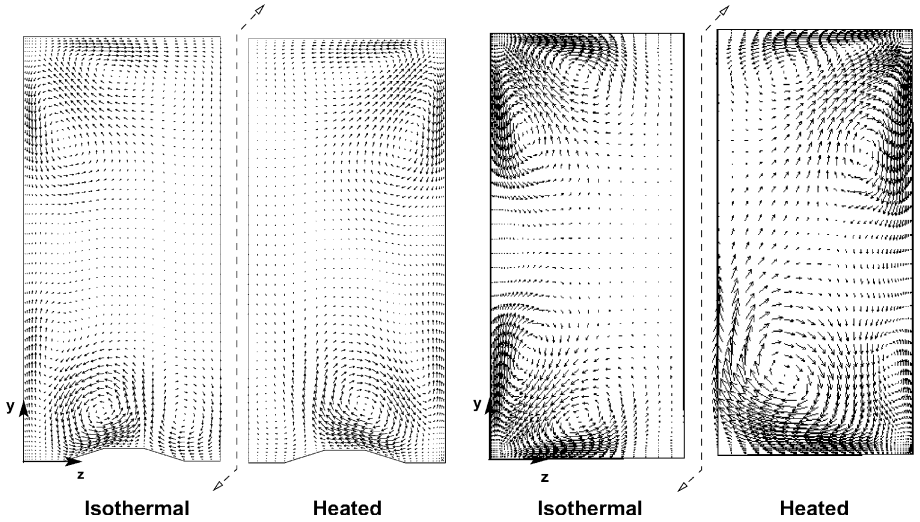

Fig. 8. Secondary flows in isothermal (left) and heated (right) square duct.

Table 4
Heated ridged ducts (maximal transversal velocity for BSF and SSF)

Type of duct	BSF	SSF
Square duct	2.9% U_b	–
Trapezoidal ridged	3.5% U_b	0.5% U_b
Triangular ridged	3.4% U_b	0.25% U_b
Circular ridged	3.3% U_b	≈0

duced by the lateral wall are such that the ejections can only take place in the vicinity of the ducts middle plane [1]. In the ridged duct, turbulent structures are also confined by ridges, leaving a larger zone where ejections can take place. Fig. 8 compares the mean secondary flow vectors, in one half of the duct section, for the isothermal and heated cases. In the square duct, the size and intensity of the mean secondary flows increase when heating is also increased. For the heated ridged duct the mean secondary flows BSFs size is not significantly increased. The enhancement of the mean secondary flows intensity, in comparison with isothermal cases, is presented in Table 4. This increase is just ≈10% for ridged ducts, and for the square duct it is more than 50%. The SSF intensity is decreased, and in the case of the circular ridged duct SSF are not generated. The triangular and circular ridges exhibit a low limitation effect on the size of mean secondary flows.

As found in the square duct, stronger ejections in ridged ducts tend to generate more turbulent activity in the outer part of the boundary layer. However, in ridged ducts maximal turbulent activity is not concentrated in the middle wall plane as it is in heated square ducts. This zone extends from the middle wall plane ($z/D_h = 0.5$) to the middle ridged plane ($z/D_h = 0.25$). Fig. 9 shows the contours of the Reynolds stress $\langle u'v' \rangle$ for the cases studied. The trapezoidal ridge presents a more extended $\langle u'v' \rangle$ maximal zone. The maximal $\langle u'v' \rangle$ zone for the other two ridges is more concentrated in the middle wall plane. As in isothermal ridged ducts, evolu-

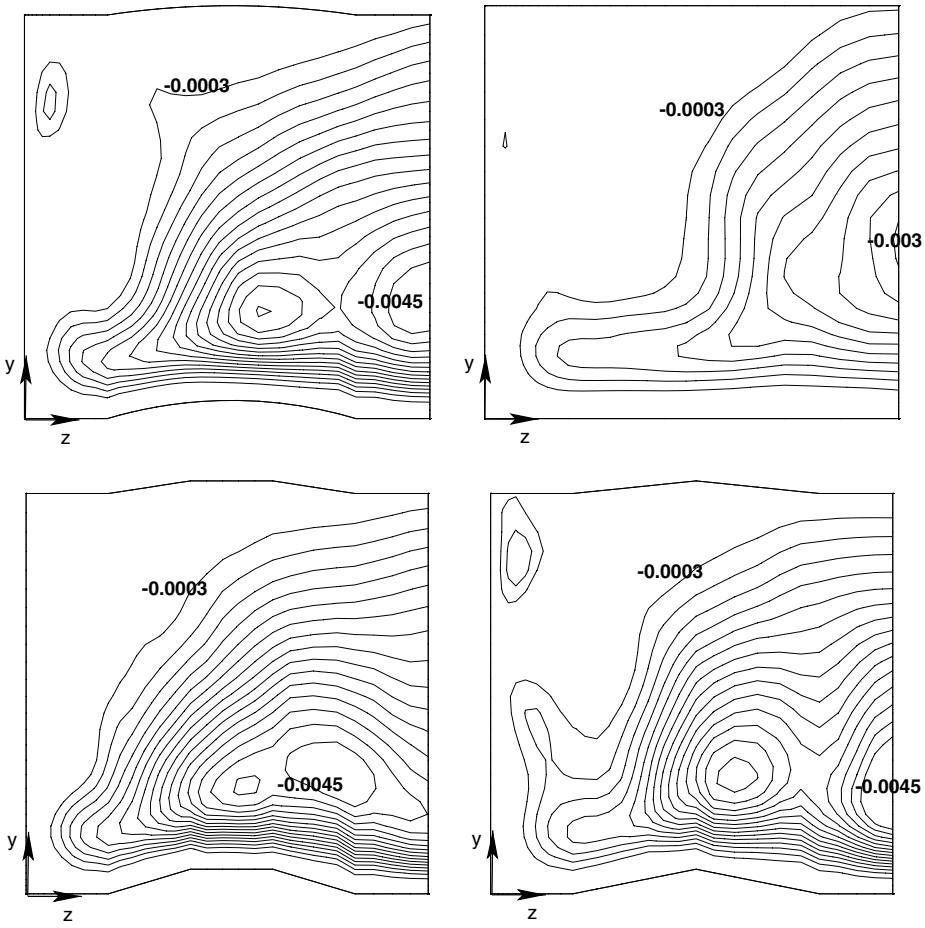

Fig. 9. Contours of Reynolds stresses $\langle u'v' \rangle$. Values normalized by U_b^2. Step $-0.0003\langle u'v' \rangle / U_b^2$. 1/4 transversal section.

tion in function of the ridge form of u_{rms} is not present. Ridges have no fundamental influence on the streamwise velocity fluctuations.

Finally Table 5 provides the mean bulk values of skin friction (C_f^{α}) and wall heat transfer (q_w^{α}) above the ridged wall. It assesses the increment of these parameters, vis-à-vis the heated square duct. The trapezoidal ridge induces the most important increase for both variables. The stronger mean secondary flows in this ridged wall enhance thermal performance, albeit they also induce additional viscous looses.

5.1. Wall turbulent structures

When one of the four walls of a square duct is heated, the increase of viscosity with temperature is followed by an enhancement of the viscous length δ^l [1], over the whole heated wall. It was established in [1] that the width of low- and high-speed streaks scales with the viscous thickness, and this is verified as seen in Fig. 10. However, when the width of these streaks is normalized by the viscous thickness δ^l, values obtained in the isothermal case are very close to those obtained in the heated cases [1] e.g $\lambda^+ \approx 100$.

The limitation in size and intensity produced by ridges in the mean secondary flows is also reflected in the low- and high-speed streaks. The width increase of these structures in a heated duct, similarly to the mean secondary flows, is not well defined. Fig. 11 shows instantaneous contours of streamwise velocity fluctuations for both the isothermal and heated trapezoidal ridged duct. The enhancement in length and diameter of streaky structures and the concentration of a low-speed streak structure, related to the strong ejections, around the middle wall plane are not observed. These weak changes in comparison with the isothermal duct, avoid the concentration of turbulence in a small zone. Because a mixing effect is located in a larger zone, a higher thermal performance than in the square ducts is found in the case of ridged ducts.

Table 5
Heated ridged duct (skin friction, C_f and normal to wall heat transfert, q_w, increase)

Type of duct	C_f^{α} (%)	q_w^{α} (%)
Trapezoidal ridged	+7.9	+11.3
Triangular ridged	+5.1	+5.3
Circular ridged	+7.7	+7.9

5.2. Turbulent heat transfer

Turbulent heat transfer is linked to turbulent phenomena as ejections, which transport hot fluid from a

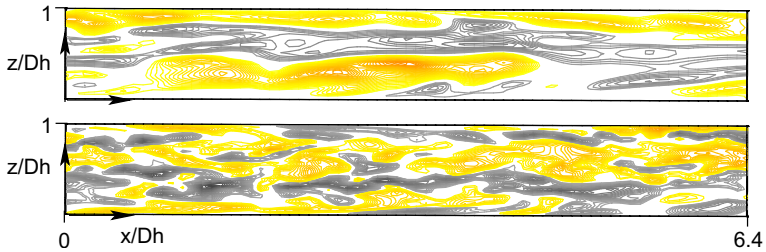

Fig. 10. Isolines of fluctuant streamwise velocity in heated square duct (top) (plan (x,z) at $y^+ = 13$) and in isothermal square duct (bottom) (plan (x,z) at $y^+ = 16$). Dark isolines represent low speed streaks ($-0.5 < u' < 0.0$) and grey isolines represent high speed streaks ($0.0 < u' < 0.5$). Step $-0.0003\langle u'v'\rangle/U_b^2$. 1/4 transversal section, grey isolines represent high speed streaks ($0.0 < u < 0.5$).

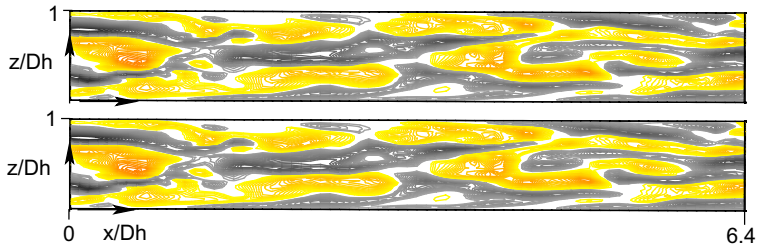

Fig. 11. Isolines of fluctuant streamwise velocity in heated trapezoidal ridged duct (top) (plan (x,z) at $y^+ = 14$) and in isothermal trapezoidal ridged duct (bottom) (plan (x,z) at $y^+ = 19$). Dark isolines represent low speed streaks ($-0.5 < u < -0.0$) and grey isolines represent high speed streaks ($0.0 < u < 0.5$).

heated wall towards the duct core, as well as to sweeps that bring back cold fluid to the heated wall [16]. The turbulent heat transfer is effected by the correlation $\langle \vec{u}'T' \rangle$, whose three components are: $\langle u'T' \rangle$, $\langle v'T' \rangle$ and $\langle w'T' \rangle$.

The hierarchy between different forms of ridges concerning the increase of turbulent heat flux is totally coherent with the hierarchy concerning the increase of turbulent activity provided in Fig. 9. The trapezoidal ridge duct induces a 200% increase in $\langle u'T' \rangle$ and more than 100% in $\langle v'T' \rangle$ over the ridges, when compared to a square duct. For all ridged ducts, the streamwise component $\langle u'T' \rangle$ of the turbulent heat transfer reaches a maximum between the middle of each ridge, $z/D_h = 0.25$ and the middle wall plane, $z/D_h = 0.5$, see Fig. 12. However, $\langle v'T' \rangle$ maximum values, for circular and triangular ridges, are concentrated around the middle plane duct, see Fig. 13. This effect is not observed in the trapezoidal ridged ducts where the $\langle v'T' \rangle$ maximum value is as high as those in the other ducts, but it is extended to a larger area, thus increasing the thermal performance of such ridged duct, see Fig. 13. This result indicates that small turbulent structures have a higher thermal efficiency than the big structures created in the heated square duct. Thermal performances is then related to the capacity of a ridge to limit the turbulent structure size, while conserving its magnitude.

6. Influence of ridges position and height

As previously discussed, thermal performance improvement ascribed to the ridge-flow interaction is mainly related to the increase of turbulent activity. Considering the results presented herewith, it would be expected that the ridges induce the following characteristics: limitation in size of turbulent structures, maximum turbulent activity in an extended zone, maximum fluctuating temperature in an extended zone, and an increase of the mean wall heat transfer with minimum viscous loss.

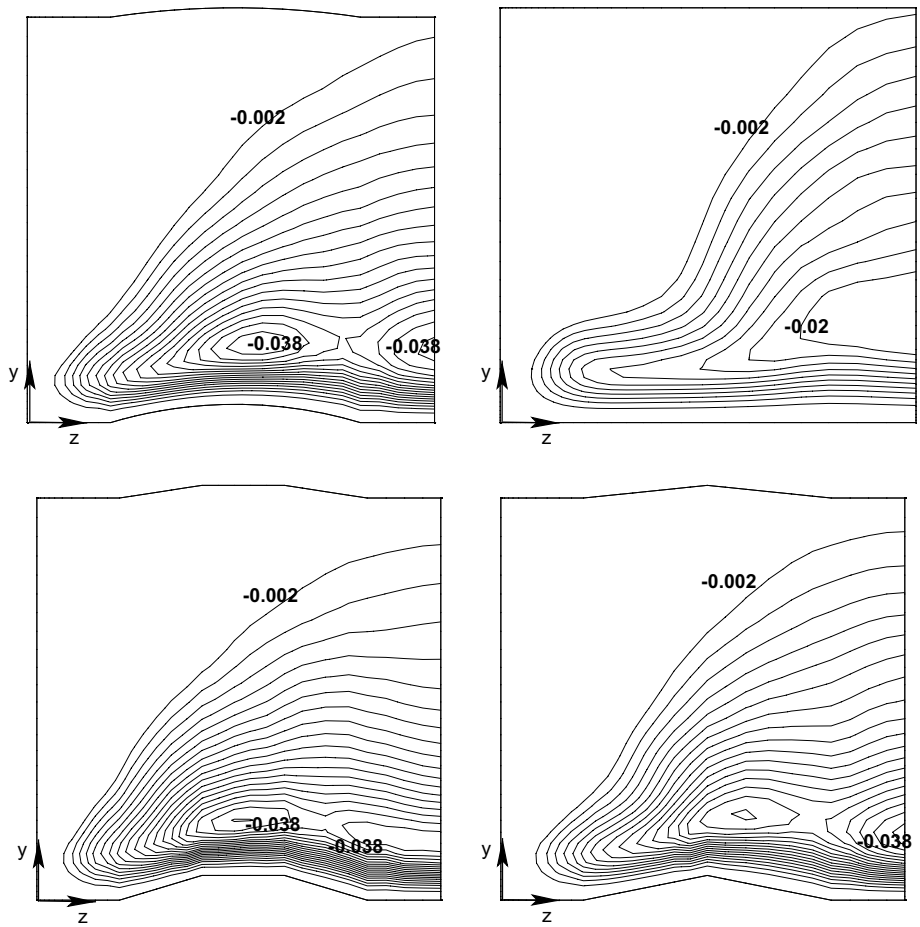

Fig. 12. Contours of $\langle u'T' \rangle$. Values normalized by $T_w U_b$. Step $-0.002\langle u'T' \rangle / T_w U_b$. 1/4 transversal section.

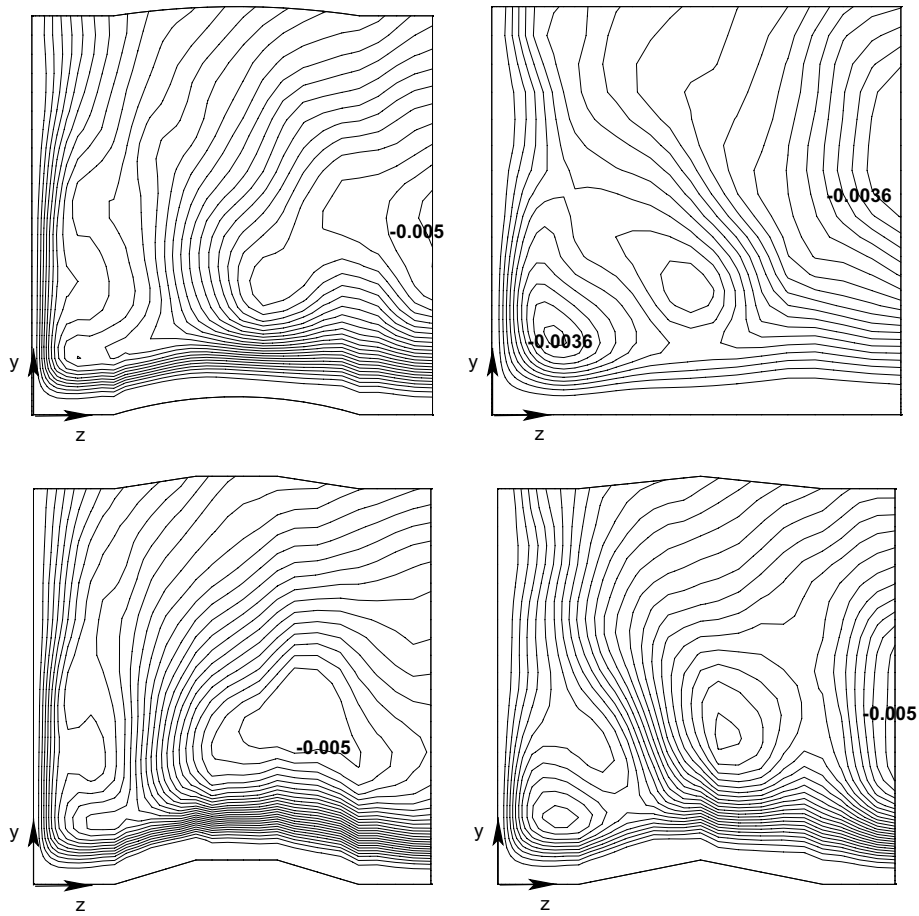

Fig. 13. Contours of $\langle v'T' \rangle$. Values normalized by $T_w U_b$. Step $-0.0005\langle v'T' \rangle / T_w U_b$. 1/4 transversal section.

As shown in this investigation, the trapezoidal ridge is the best geometry to enhance thermal performance. In this section, we briefly study the effect of the ridge position and ridge height on turbulent flow behavior. Table 6 presents the characteristics of three different trapezoidal ridges. In all cases, the temperature applied to the ridged wall still correspond to the ratio $T_h/T_w = 2.5$. Case0 is the one described in the previous sections.

The transverse velocity field vector shows the size and the form of the mean secondary flows. For case1, where ridges are closer to the lateral walls, the mean secondary flows *jump* at the ridge. An inclined larger secondary flow is then induced, with strong turbulent activity that is manifest in a less extended zone. Thermal and turbulent advantages observed in the previous section are then lost. The maximum amplitude for the fluctuating temperature is decreased by ≈20% with respect to case0.

A similar behavior is observed for case2. The $\langle u'v' \rangle$ maximum value contours are concentrated over the ridge than in case1. The maximum T_{rms} values are also concentrated over the ridge. For both cases a weak decrease (from 5% to 10% with respect to case0) of the wall heat transfer is observed.

Table 6
Heated ridged duct (trapezoidal ridges geometrical characteristics)

Form	H/D_h	B/D_h	b/D_h	I/D_h
Case0	0.03	0.3	0.1	0.5
Case1	0.03	0.3	0.1	0.6
Case2	0.03	0.3	0.1	0.4
Case3	0.05	0.3	0.1	0.5

Case3 shows a BSF similar in form but stronger in intensity than case0. The maximum transverse velocity is $\approx 4\% U_b$. An increase of the maximum $\langle u'v' \rangle$ values ≈15% with respect to case0 is observed. This zone is also concentrated over the ridges. The turbulent thermal activity is enhanced in comparison with the previous

cases, the maximum T_{rms} value is almost 35% greater than in case0 and more than 50% when compared to the other cases. Indeed, thermal performance enhancement for this case3, is also coincident with an increase in viscous losses by 10% with respect to case0 (Fig. 14).

7. Conclusion

The present paper investigates the importance of duct transverse geometry on turbulent flow behavior, and its close relationship to the creation of secondary flows.

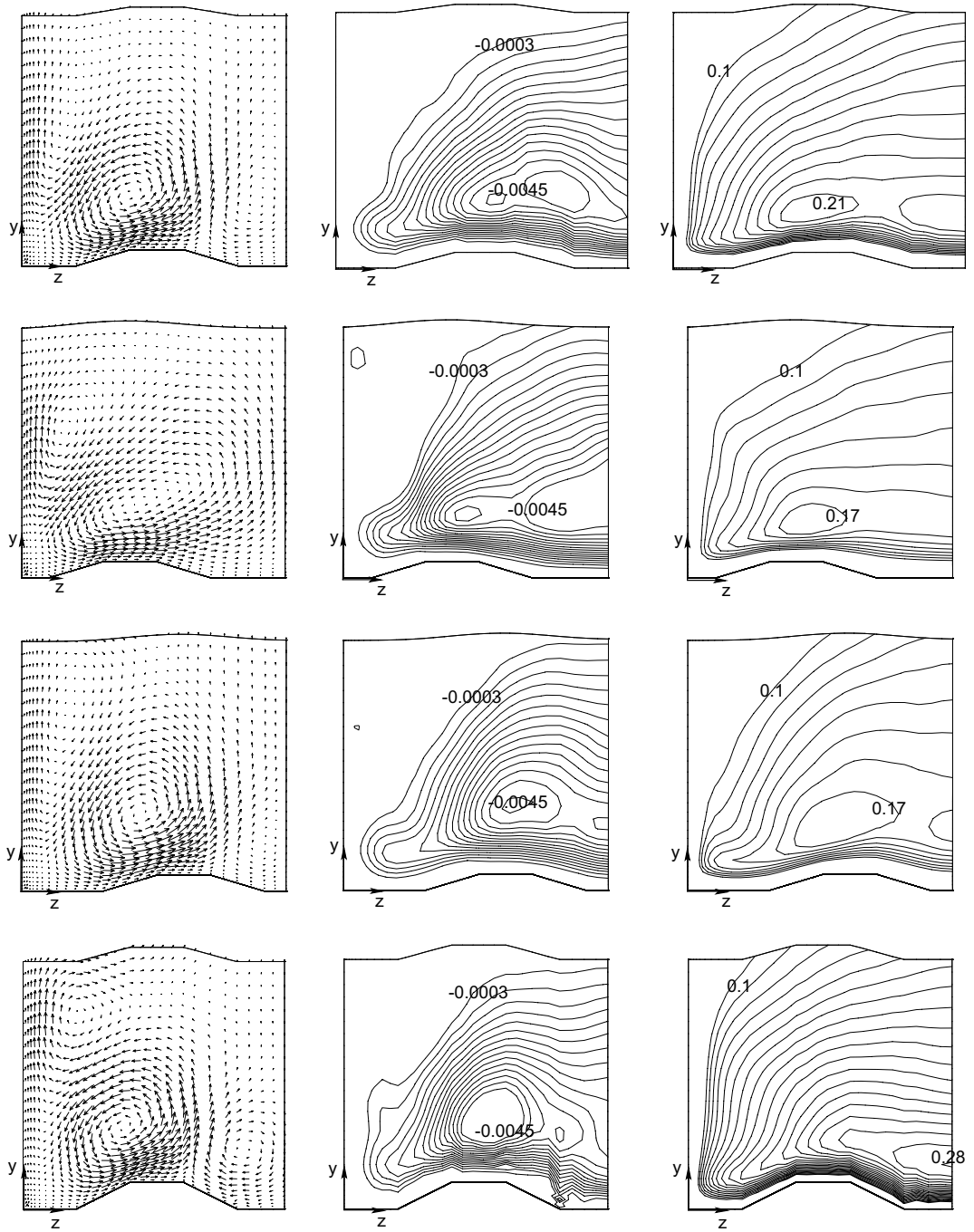

Fig. 14. (Left) Mean secondary flows vectors. (Middle) Contours of $\langle u'v' \rangle$. Values normalized by U_b^2. Step $-0.0003\langle u'v' \rangle / U_b^2$. (Right) Contours of T_{rms}. Values normalized by T_w. Step $0.1T_{rms}/T_w$. 1/4 transversal section.

The introduction of small ridges induces important changes in turbulent flow behavior. Fluctuations of the normal to the wall velocity component (the most affected velocity component by the ridges) are enhanced, in some cases by more than 100% of the value found in an unridged square duct. Ridges induce an enhancement of the Reynolds stresses $\langle u'v' \rangle$ due to the increase of ejections over them. In future works, a dynamic procedure for the local Prandtl number must be added to the numerical simulation, due to the strongly anisotropic flow behavior. Several thermal benefit effects of ridges are emphasized: increase of thermal turbulent activity and turbulent heat transfer, increase of the global normal to the wall heat transfer by the creation of new secondary flows (SSF) and the decrease of the wall turbulent structures size by the confining ridges. This last point is very important, because it means that large turbulent structures created by the dilatation of the viscous width in heated plane walls have a weak thermal performance. The placement of ridges limits the width of turbulent structures, and increases the global thermal performance of the duct. These advantages notwithstanding, viscous losses are also enhanced. Similar effects were observed in ribblets works, which constitute a significant negative point for practical purposes. The last results allows a choice for the best geometry, considering the balance between the viscous losses and the increase in thermal performance.

We consider that the best ridge geometry, from among the three studied herein, is the trapezoidal one. However, when ridges are moved toward the lateral wall or toward the middle wall plan, ridges partially loose the thermal performance enhancement. This implies that the thermal performance of ridges is not only function of the increase of the secondary flow intensity but are also a function of their size control.

Acknowledgments

This research was supported by the Centre National d'Etudes Spatiales (CNES, France) and MoST team in the Institut National Polytechnique de Grenoble, France. Computations were carried out at the Institut du Développement et des Ressources en Informatique Scientifique (IDRIS, France). First author acknowledges the *Universidad Nacional Autónoma de México* (UNAM, *México*) and *Secretaría de Educación Pública de México* (SEP, *México*) for financial support.

References

[1] M. Salinas Vázquez, O. Métais, Large eddy simulation of the turbulent flow through a heated square duct, J. Fluid Mech. 453 (2002) 201–238.
[2] O. Métais, M. Lesieur, New trends in large eddy simulations of turbulence, Ann. Rev. Fluid Mech. 28 (1996) 45–82.
[3] E. David, Modélisation des écoulements compressibles et hypersoniques: Une approche instationnaire. PhD Theses, Institut National Polytechnique de Grenoble, France, 1993.
[4] O. Métais, M. Lesieur, Spectral large eddy simulation of isotropic and stably-stratified turbulence, J. Fluid Mech. 239 (1992) 157–194.
[5] D. Gottlieb, E. Turkel, Dissipative two four methods for time-dependent problems, Math. Comp. 30 (1976) 703–723.
[6] S. Gavrilakis, Numerical simulation of low Reynolds number turbulent flow through a straight square duct, J. Fluid Mech. 244 (1992) 101–112.
[7] A. Huser, S. Biringen, Direct numerical simulation of turbulent flow in a square duct, J. Fluids Mech. 257 (1993) 65–95.
[8] A. Demuren, W. Rodi, Calculation of turbulence-driven secondary motion in noncircular ducts, J. Fluid Mech. 140 (1984) 189–222.
[9] F.B. Gessner, J.B. Jones, On some aspects of fully developed turbulent flow in a rectangular channel, J. Fluids Mech. 23 (1965) 689–713.
[10] F.B. Gessner, The origin of secondary flow in turbulent flow along a corner, J. Fluids Mech. 58 (1983) 1–23.
[11] D.B. Goldstein, T.C. Tuan, Secondary flow induced by ribletsi, J. Fluid Mech. 363 (1998) 115–151.
[12] I. Nezu, H. Nakagawa, Cellular secondary currents in straight conduit, J. Hydr. Eng. 110 (1984) 173–193.
[13] S.J. McLelland, J.A. Phillip, J.L. Best, J.R. Livesey, Turbulence and secondary flow over sediment strips in weakly bimodal bed material, J. Hydr. Eng. 125 (1985) 463–473.
[14] L. Falconer, V. Armenio, Large eddy simulation of secondary flow over longitudinally-ridged walls, J. Turbul. 3 (2002) 008.
[15] H. Kawamura, T. Sumori, DNS of turbulent flow in a channel with longitudinally ridged walls, in: P.R. Voke, N.D. Sandham, L. Kleiser (Eds.), Direct and Large Eddy Simulation, vol. III, Kluwer Academic Publ., 1999, pp. 405–416.
[16] M. Salinas Vázquez, W. Vicente Rodríguez, Efecto de estructuras turbulentas no estacionarias sobre la térmica de flujos en conductos de sección cuadrada con un flujo de calor no simétrico. Rev. Sociedad Mexicana de Física, accepted for publication.